Published by Institute of Physics Publishing for SISSA
Received: *July 24, 2007*
Revised: *November 7, 2007*
Accepted: *November 27, 2007*
Published: *December 12, 2007*

T-odd asymmetries in radiative top-quark decays

Kaoru Hagiwara
KEK Theory Division and Sokendai,
Tsukuba 305-0801, Japan
E-mail: kaoru.hagiwara@kek.jp

Kentarou Mawatari
School of Physics, Korea Institute for Advanced Study,
Seoul 130-722, Korea
E-mail: kentarou@kias.re.kr

Hiroshi Yokoya[*]
Department of Physics, Niigata University,
Niigata 950-2181, Japan
E-mail: yokoya@nt.sc.niigata-u.ac.jp

Abstract: We study the angular distribution of the charged lepton in the top-quark decay into a bottom quark and a W boson which subsequently decays into $\ell\nu_\ell$, when a hard gluon is radiated off. The absorptive part of the $t \to bWg$ decay amplitudes, which gives rise to T-odd asymmetries in the distribution, is calculated at the one-loop level in perturbative QCD. The asymmetries at a few percent level are predicted, which may be observable at future colliders.

Keywords: Space-Time Symmetries, Heavy Quark Physics, NLO Computations, QCD.

[*]Address from December 1, 2007: Theory Unit, Physics Department, CERN, CH-1211 Geneva 23, Switzerland; E-mail: hiroshi.yokoya@cern.ch

http://jhep.sissa.it/archive/papers/jhep122007041/jhep122007041.pdf

JHEP12(2007)041

Contents

1. Introduction

T-odd effects in hard QCD processes have been attracting our attentions for more than 30 years, but no experimental verification of the predictions [1−9] has been presented yet. T-odd observables change sign under the operation of reversing both the spatial momenta and the spins of the all the particles without interchanging initial and final states; see refs. [10, 4] for details.[1] In T-invariant theories like perturbative QCD, the T-odd effects arise due to the re-scattering phase, or the absorptive part of the amplitudes, which appears in the loop level. Such T-odd quantities in hard processes can be predicted in perturbative QCD, and should be tested experimentally.

Since de Rújula et al. proposed to measure T-odd effects as an experimental test of the non-abelian nature of QCD in $e^+e^- \to \Upsilon \to ggg$ with a longitudinally polarized beam [1], several theoretical studies have been performed for the quark and gluon processes with an electroweak current. They can be classified into three types:

1. Three jets in e^+e^- annihilation with a longitudinally polarized beam, $e^+e^- \to q\bar{q}g$ [2, 7, 9].

[1] T-odd effects are sometimes referred to as naïve-T-odd [11] or T_N-odd [9] in order to distinguish them from the genuine time-reversal operation T, which exchanges the initial and the final states.

2. Semi-inclusive deep-inelastic neutrino [3] or longitudinally polarized electron [4, 12] scattering, $\ell p \to \ell' h X$.

3. Drell-Yan-type process, $p\bar{p} \to \gamma^*/W/Z + \mathrm{jet} + X$. References [5, 13, 14] considered single-spin asymmetry in the Drell-Yan process with longitudinally polarized proton beam, while T-odd effects without spin measurement were studied in W-jet [6, 11] and Z-jet [8] events at hadron colliders.

The absorptive parts of the relevant one-loop amplitudes in these three processes are related to each other through crossing [15]. In addition to above three processes, there also exists another T-odd observable, the normal polariation in top-quark pair-production at e^+e^- and hadron colliders [16 − 21].

Observations of T-odd effects in hard processes are a challenging task since they do not appear at the tree level. So far, no experimental test has been made for the above processes [22 − 24], even though large non-perturbative T-odd effects have been observed in hadron spin physics [23, 25]. We may note that the possibility to observe the perturbative T-odd effects in W-jet events at the Tevatron run II has recently been pointed out in [11].

In this article, we propose a new measurement of the T-odd effects in radiative top-quark decays. We study T-odd angular distributions of W-decay leptons in the radiative top-quark decay into a bottom quark, a W boson, and a gluon:

$$t \to b + W^+ + g; \quad W^+ \to \ell^+ + \nu_\ell. \tag{1.1}$$

Due to the large mass, $m_t = 175$ GeV, top-quark decay is not affected by hadronization, and hence it can be dictated by perturbative QCD. Even though the correction up to $\mathcal{O}(\alpha_s^2)$ to the total decay width of the top quark is known [26], the correction to the W-decay lepton angular distribution in the top quark decay has been calculated only up to $\mathcal{O}(\alpha_s)$ [27]. We calculate the absorptive part of the amplitudes for the $t \to bWg$ process in the one-loop order $\mathcal{O}(\alpha_s^2)$, which gives the leading contribution to the T-odd asymmetries. The predictions may be tested at future colliders such as the Large Hadron Collider (LHC) and the International Linear Collider (ILC).

The article is organized as follows. In section 2, we present the lepton decay distribution using the density matrices of the $t \to bWg$ decay and the $W \to \ell\nu$ decay, and give the general kinematics relevant to our analysis. In section 3, after showing the T-even lepton angular distributions, we discuss the T-odd distributions in detail, and study their observability at future experiments. In section 4, we consider radiative decays of polarized top-quarks and discuss another T-odd observable, the angular correlation between the top-quark spin and the decay plane. Section 5 is devoted to a summary. In appendix A, we give the absorptive part of the $t \to bWg$ decay amplitudes in the one-loop order by using the Feynman parameter integral calculation. In appendix B, we present our results in terms of the loop scalar functions.

2. $t \to bW^+g$ decay density matrix

The decay rate of the process (1.1) can be expressed in terms of the $t \to bWg$ decay and

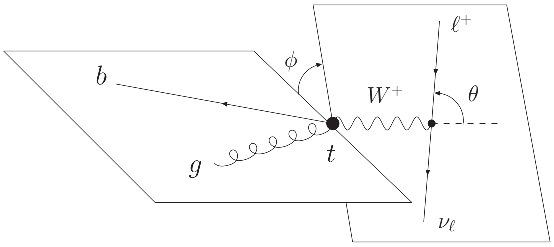

Figure 1: Schematic view of the coordinate system for the $t \to bW^+g$ decay, followed by the $W^+ \to \ell^+\nu_\ell$ decay.

the $W \to \ell\nu$ decay density matrices in the narrow width approximation of the W boson,

$$d\Gamma = \sum_{\lambda,\lambda'} d\Gamma^t_{\lambda\lambda'} \frac{1}{\Gamma_W} d\Gamma^W_{\lambda\lambda'}, \tag{2.1}$$

where Γ_W is the total decay width of W boson, and λ, $\lambda' = \pm$, 0 denote the W-boson helicity. The 3×3 W-polarization density matrix for the W^+ decay reads

$$\frac{1}{\Gamma_W} \frac{d\Gamma^W_{\lambda\lambda'}}{d\cos\theta\, d\phi} = B_\ell \frac{3}{8\pi} L_{\lambda\lambda'}(\theta,\phi) \tag{2.2}$$

with the decay branching fraction $B_\ell = B(W \to \ell\nu)$ and

$$L_{\lambda\lambda'}(\theta,\phi) = \begin{pmatrix} \frac{(1+\cos\theta)^2}{2} & \frac{\sin\theta(1+\cos\theta)}{\sqrt{2}} e^{i\phi} & \frac{\sin^2\theta}{2} e^{2i\phi} \\ \frac{\sin\theta(1+\cos\theta)}{\sqrt{2}} e^{-i\phi} & \sin^2\theta & \frac{\sin\theta(1-\cos\theta)}{\sqrt{2}} e^{i\phi} \\ \frac{\sin^2\theta}{2} e^{-2i\phi} & \frac{\sin\theta(1-\cos\theta)}{\sqrt{2}} e^{-i\phi} & \frac{(1-\cos\theta)^2}{2} \end{pmatrix}. \tag{2.3}$$

Here, the 3×3 matrices are for λ, $\lambda' = (+, 0, -)$, and the polar and azimuthal angles (θ, ϕ) of the charged lepton are defined in the rest frame of the W boson, where the z-axis is taken along the W momentum direction in the rest frame of the top quark. The x-axis ($\theta = \pi/2$, $\phi = 0$) is in the $t \to bWg$ decay plane as explained below.

Before we show the $t \to bWg$ density matrix $d\Gamma^t_{\lambda\lambda'}$, we define the kinematical variables for the process

$$t(p_t, \sigma_t) \to b(p_b, \sigma_b) + W^+(q, \lambda) + g(p_g, \sigma_g), \tag{2.4}$$

where the four-momenta of each particle are defined in the top rest frame as

$$\begin{aligned} p_t^\mu &= (m_t, 0, 0, 0), \\ p_b^\mu &= (E_b, p_b \sin\hat{\theta}, 0, p_b \cos\hat{\theta}), \\ q^\mu &= (E_W, 0, 0, q), \\ p_g^\mu &= (E_g, p_{g,x}, 0, p_{g,z}). \end{aligned} \tag{2.5}$$

Helicities of each particle, σ_t, σ_b, λ and σ_g, are also defined in the top rest frame. The z-axis is taken along the W boson momentum, and y-axis is along $\vec{q} \times \vec{p}_b$, the normal of the decay plane; see figure 1.

JHEP12(2007)041

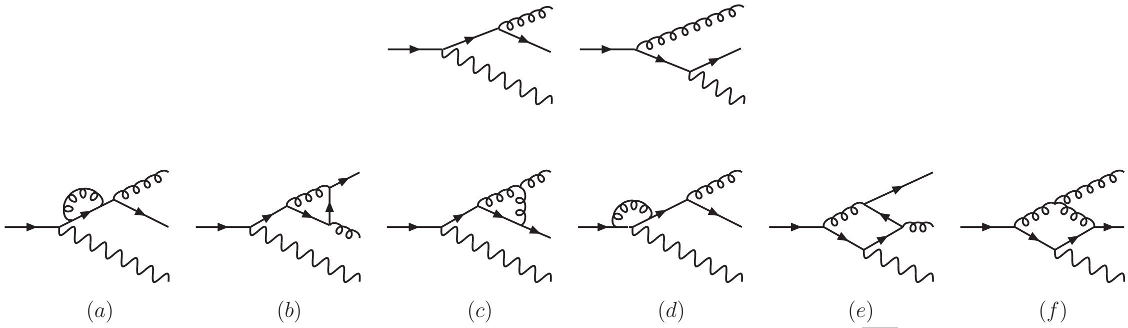

Figure 2: Feynman diagrams for the $t \to bWg$ decay [30]. The top two are the tree level diagrams, and the bottom six are the one-loop level diagrams contributing to the absorptive part of the amplitudes.

We define the dimensionless variables as

$$(z_1, z_2, z_3) \equiv \left(\frac{2p_t \cdot p_b}{m_t^2}, \frac{2p_t \cdot q}{m_t^2}, \frac{2p_t \cdot p_g}{m_t^2} \right) = \left(\frac{2E_b}{m_t}, \frac{2E_W}{m_t}, \frac{2E_g}{m_t} \right). \tag{2.6}$$

These are the energy fraction of b, W and g, respectively, and satisfy the energy conservation condition, $z_1 + z_2 + z_3 = 2$. The kinematically allowed region is given in the (z_1, z_2) plane by

$$\begin{gathered} 2y \leq z_1 \leq 1 - x^2 + y^2, \quad 2x \leq z_2 \leq 1 + x^2 - y^2, \\ (z_1^2 - 4y^2)(z_2^2 - 4x^2) - \left[2 + 2x^2 + 2y^2 - 2z_1 - 2z_2 + z_1 z_2\right]^2 \geq 0, \end{gathered} \tag{2.7}$$

with $x = m_W/m_t$ and $y = m_b/m_t$.

The mass of the b-quark is kept to be finite ($m_b = 4\,\text{GeV}$) for the tree-level calculation. However, as we will see later, the effect of the mass is negligible. Thus, for the calculation of the T-odd distributions, we take the $m_b = 0$ limit, which simplifies the framework of the one-loop calculation. In the case that we ignore the b-quark mass, there appears a kinematical singularity in the $z_2 \to 1 + x^2$ limit, when the b-quark and gluon momenta are collinear. An infra-red (IR) singularity also exists at $z_3 \to 0$, where the emitted gluon becomes soft.

Let us now present the density matrix for the $t \to bWg$ decay, $d\Gamma^t_{\lambda\lambda'}$ in eq. (2.1). The matrix elements of the $t \to bWg$ decay are expressed as

$$i\mathcal{M}_\lambda = \frac{-igg_s}{\sqrt{2}} t^a V_{tb}\, \bar{u}(p_b, \sigma_b)\, T^{\mu\alpha}\, u(p_t, \sigma_t)\, \epsilon^*_\mu(q, \lambda)\, \epsilon^{a*}_\alpha(p_g, \sigma_g), \tag{2.8}$$

where g and g_s are the weak and strong coupling constants, t^a is the SU(3) color matrix, and V_{tb} is the Cabibbo-Kobayashi-Maskawa (CKM) matrix element. The tensor $T^{\mu\alpha}$ is a 4×4 matrix in the spinor space. The leading contribution to the real part of $T^{\mu\alpha}$ comes from the tree diagrams [28, 29], while the imaginary part appears first in the one-loop diagrams. All the tree and the one-loop diagrams needed in our analysis are shown in figure 2. We give details of our calculation of $T^{\mu\alpha}$ in the appendices.

JHEP12(2007)041

Factorizing the color factor and the coupling constants, we define the reduced density matrix $H_{\lambda\lambda'}$ as

$$\overline{\sum}\mathcal{M}_\lambda\mathcal{M}^*_{\lambda'} = 4\sqrt{2}\pi G_F\alpha_s m_W^2|V_{tb}|^2C_F\cdot H_{\lambda\lambda'}. \tag{2.9}$$

The summation stands for the sum/average of the spins of the particles except W boson and the sum/average of colors. In terms of $H_{\lambda\lambda'}$, the density matrix $d\Gamma^t_{\lambda\lambda'}$ is expressed as

$$\frac{d\Gamma^t_{\lambda\lambda'}}{dz_1dz_2} = \frac{G_F\alpha_s m_t^3x^2|V_{tb}|^2C_F}{32\sqrt{2}\pi^2}H_{\lambda\lambda'}(z_1,z_2). \tag{2.10}$$

Finally, combining the top- and W-decay density matrices in eqs. (2.10) and (2.2), the decay distribution in eq. (2.1) is expressed as

$$\begin{aligned}\frac{d\Gamma}{dz_1dz_2\,d\cos\theta\,d\phi} =& \frac{3B_\ell G_F\alpha_s m_t^3x^2|V_{tb}|^2C_F}{256\sqrt{2}\pi^3}\sum_{\lambda,\lambda'}H_{\lambda\lambda'}(z_1,z_2)\,L_{\lambda\lambda'}(\theta,\phi) \\ \equiv& K\big[F_1(1+\cos^2\theta)+F_2(1-3\cos^2\theta)+F_3\sin 2\theta\cos\phi+F_4\sin^2\theta\cos 2\phi \\ &+F_5\cos\theta+F_6\sin\theta\cos\phi+F_7\sin\theta\sin\phi+F_8\sin 2\theta\sin\phi+F_9\sin^2\theta\sin 2\phi\big],\end{aligned} \tag{2.11}$$

where K is the factor in front of the summation symbol in the first line. The nine independent functions $F_{1-9}(z_1,z_2)$ are defined in terms of the reduced density matrices $H_{\lambda\lambda'}$ as

$$\begin{aligned}
F_1 &= \frac{1}{2}\left(H_{++}+H_{00}+H_{--}\right), & F_6 &= \frac{1}{\sqrt{2}}\left(H_{+0}+H_{0+}+H_{-0}+H_{0-}\right),\\
F_2 &= \frac{1}{2}H_{00}, & F_7 &= \frac{i}{\sqrt{2}}\left(H_{+0}-H_{0+}-H_{-0}+H_{0-}\right),\\
F_3 &= \frac{1}{2\sqrt{2}}\left(H_{+0}+H_{0+}-H_{-0}-H_{0-}\right), & F_8 &= \frac{i}{2\sqrt{2}}\left(H_{+0}-H_{0+}+H_{-0}-H_{0-}\right),\\
F_4 &= \frac{1}{2}\left(H_{+-}+H_{-+}\right), & F_9 &= \frac{i}{2}\left(H_{+-}-H_{-+}\right).\\
F_5 &= H_{++}-H_{--}, & &
\end{aligned} \tag{2.12}$$

The terms independent of the azimuthal angle, F_1, F_2 and F_5, are provided from the diagonal terms of the density matrix, while the azimuthal-angle dependent terms are provided from the off-diagonal terms, i.e. the interference between the different polarization states of the W boson. The terms F_1 through F_6 are T-even, and the leading contribution comes from the tree diagrams. On the other hand, F_7 to F_9 are T-odd, and they receive the leading contribution from the absorptive part of the one-loop amplitudes through the interference with the tree amplitudes. Parity transformation changes the sign of ϕ, thus $F_{7,8,9}$ are not only T-odd but also parity-odd (P-odd). Assuming CP invariance, the lepton angular distribution for the anti-top-quark decay, $\bar{t}\to\bar{b}W^-g$; $W^-\to\ell^-\bar{\nu}_\ell$, can be obtained by changing the sign of $F_{7,8,9}$ in eq. (2.11).

3. Lepton decay distributions

In this section, we present numerical results for the T-even and T-odd lepton angular distributions in radiative top-quark decays. Note that, in our leading-order analysis, the T-even distributions F_{1-6} are $\mathcal{O}(\alpha_s)$, while T-odd distributions $F_{7,8,9}$ are $\mathcal{O}(\alpha_s^2)$.

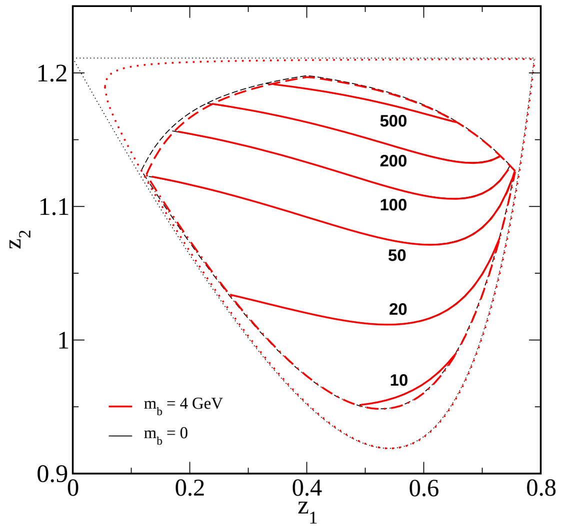

Figure 3: Contour plot of $F_1(z_1, z_2)$ in the tree level. z_1 and z_2 are the energy fraction of the bottom quark and the W boson, respectively. The dotted line denotes the kinematical boundary; the dashed and dot-dashed lines are for the kinematical cuts for $k_T > 20\,\mathrm{GeV}$ and $\cos\theta_{bg} > -0.9$, respectively. The thick contours are obtained for $m_b = 4\,\mathrm{GeV}$, whereas the thin contours are for $m_b = 0$.

3.1 T-even distributions

In figure 3, we show a contour plot of the function $F_1(z_1, z_2)$, which gives the total rate of the $t \to bWg$ decay, $d\Gamma/dz_1 dz_2 = K\,(16\pi/3)\,F_1$, after integrating over the lepton decay angles. The kinematical boundary given by eq. (2.7) for $m_t = 175\,\mathrm{GeV}$, $m_W = 80.4\,\mathrm{GeV}$ and $m_b = 4\,\mathrm{GeV}$ ($m_b = 0$) is shown by the thick (thin) dotted line. To avoid the IR region near $z_2 = z_{2\max} \sim 1.2$, we impose the k_T cut,

$$k_T^2 \equiv 2\min(p_b^2, p_g^2)\,(1 - \cos\theta_{bg}) > (20\,\mathrm{GeV})^2, \tag{3.1}$$

where θ_{bg} is the angle between the b-quark and gluon momenta in the top rest frame, shown by the dashed line. Furthermore, we apply the following cut:

$$\cos\theta_{bg} > -0.9, \tag{3.2}$$

shown by the dot-dashed line, in order to avoid the configuration where the b-quark and gluon jets are anti-collinear. These two cuts enable us to define the top decay plane spanned by $\vec{p}_b$ and $\vec{p}_g$, from which the azimuthal angle ϕ of the decay lepton is measured (see figure 1).

The decay rate is large in the region where z_2 is large, because of the collinear singularity in the $m_b = 0$ limit. As the figure shows, the effect of the b-quark mass is small for the decay-rate itself, however the kinematical boundary as well as the cuts are changed slightly by the mass.

JHEP12(2007)041

Next, we define the differential asymmetries as

$$A_i(z_2) \equiv \int dz_1\, F_i(z_1, z_2) \Big/ \int dz_1\, F_1(z_1, z_2) \tag{3.3}$$

for $i = 2$ to 9. In figure 4, we show the z_2 distributions of the T-even asymmetries $A_{2,\dots,6}$ at the tree level for the three z_1 regions: $z_{1\min} < z_1 < 0.4$, $0.4 < z_1 < 0.55$ and $0.55 < z_1 < z_{1\max}$, with the same kinematical cuts as in figure 3. The z_2 distributions of F_1 for the same z_1 regions are also shown as a reference. In all the figures, predictions for $m_b = 4\,\mathrm{GeV}$ and the massless b-quark limit are shown by thick and thin lines, respectively. Except for F_1, the lines for $m_b = 4\,\mathrm{GeV}$ and those for $m_b = 0$ are almost degenerated. Small difference in F_1 at large z_2 and small z_1 arises because of the difference in the kinematical boundary, as shown in figure 3.

The asymmetries in the polar angular distribution $A_{2,5}$ are predicted to be large, more than the azimuthal angular asymmetries $A_{3,4,6}$. When the W-boson energy (i.e., z_2) is large, the kinematics of the $t \to bWg$ three-body decays becomes close to that of the $t \to bW$ two-body decays. Near $z_2 = z_{2\max}$, this leads to the well known results: (i) The asymmetry A_2, which dictates the fraction of the decay to the longitudinally polarized W bosons, reaches 0.7. (ii) The fraction to the left-handed W bosons is ~ 0.3, and the fraction to the right-handed W bosons is negligible. This corresponds to the asymmetry $A_5 \propto H_{++} - H_{--} \sim -H_{--}$. The difference of the factor 2 comes from the normalization in eq. (2.12). (iii) The $A_{3,4,6}$ asymmetries vanish in the large z_2 region, since the interference between the different helicity states of the W boson is very small.

On the other hand, the smaller z_2 becomes, the larger the gluon contribution becomes. Due to this gluon contribution, the decay to the right-handed W boson is allowed, even in the $m_b = 0$ limit, which causes the deviation from the values in the two-body decay process.

3.2 T-odd distributions

Let us now turn to the T-odd asymmetries, the main subject of this article. As mentioned above, the leading contribution to the T-odd effects in the top-quark decay (1.1) comes from the interference between the tree diagrams and the absorptive part of the six one-loop diagrams in figure 2. The one-loop amplitudes are calculated in the $m_b = 0$ limit, however the kinematical boundary as well as the cuts are given for $m_b = 4\,\mathrm{GeV}$. We set the QCD coupling constant as $\alpha_s = \alpha_s(k_{T\min} = 20\,\mathrm{GeV}) = 0.15$. The details of our calculation of the one-loop amplitudes are given in the appendices.

Figure 5 shows the asymmetry distributions as figure 4, but for $A_{7,8,9}$ in eq. (3.3). We found that the asymmetry A_7 is positive at a few percent level, and tends to be larger with increasing z_1 and decreasing z_2. A_8 is also positive but less than 1% in magnitude, and is large for the intermediate values of z_1 and z_2. A_9 is the smallest in magnitude and is order permill. It takes positive value for large z_1 and small z_2, but changes the sign by decreasing z_1 and increasing z_2. The dips which appear in the figure are caused by the kinematical cuts given in eqs. (3.1) and (3.2).

JHEP12(2007)041

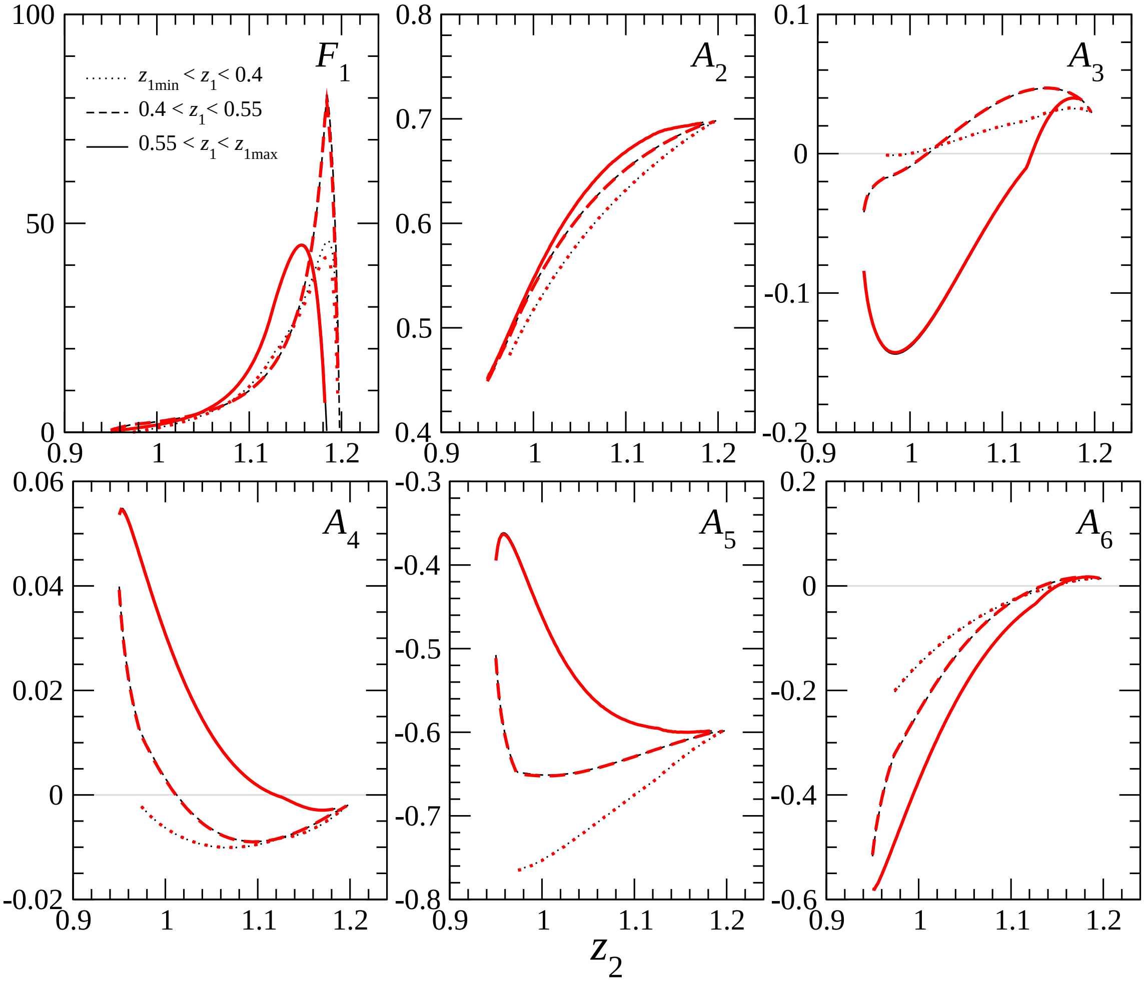

Figure 4: The z_2 distributions of the T-even asymmetries A_2 to A_6 at the tree level. Three cases for the different z_1 regions with the same kinematical cuts as figure 3 are shown. Thick lines are for $m_b = 4\,\text{GeV}$, and thin lines are for $m_b = 0$. The distributions of F_1 integrated for z_1 are also shown as a reference.

In figure 6, we show the contribution to the A_7 asymmetry for $0.55 < z_1 < z_{1\text{max}}$ from the individual one-loop diagrams of figure 2 in the Feynman gauge. The sum of the diagrams (c) and (f), which have the gluon three-point-vertex, gives negative contribution to A_7. On the other hand, all the other diagrams give positive contribution to the asymmetry. The diagrams (a) and (d) with s-channel b-quark exchange diagrams give the dominant contribution, which make the total asymmetry positive. The diagrams (b) and (e), which contain the u-channel b-quark exchange in the final-state rescattering, are found to give small contribution. On the other hand, the main contribution for A_8 comes from the diagrams $(c)+(f)$, while for A_9, the contributions from $(a)+(d)$ and $(c)+(f)$ are comparable in size.

JHEP12(2007)041

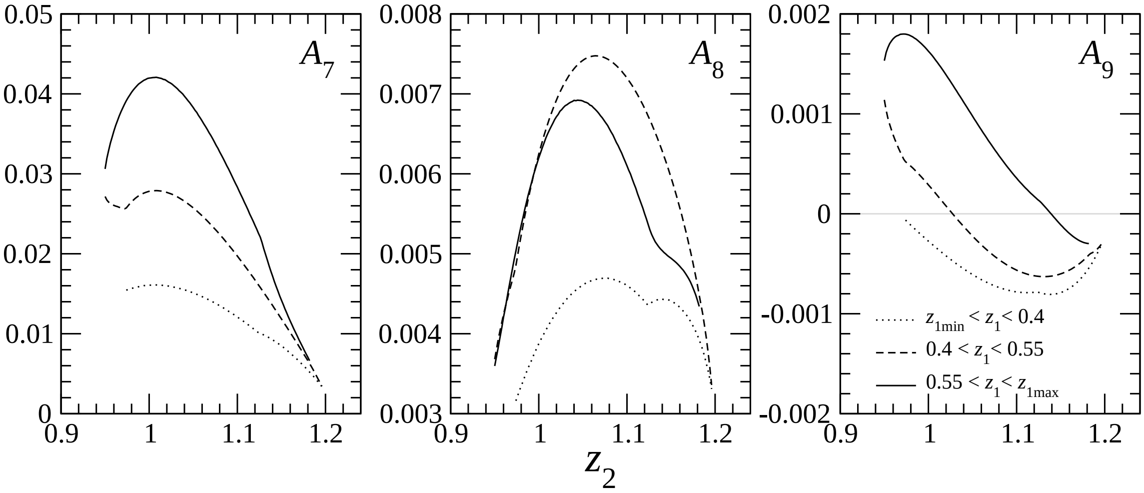

Figure 5: The same as figure 4, but for the T-odd asymmetries $A_{7,8,9}$ at the one-loop level.

3.3 Up-down asymmetry for the LHC experiment

In order to help finding an evidence of the T-odd asymmetries in experiments, we discuss a simple observable for the T-odd asymmetry. We define the up-down asymmetry $A_{\rm UD}$ with respect to the top decay plane as

$$A_{\rm UD} \equiv \left[N(0<\phi<\pi) - N(\pi<\phi<2\pi)\right]/N_{\rm sum}. \tag{3.4}$$

It is defined as the asymmetry between the number of events having the charged lepton momentum with positive and negative y component. $A_{\rm UD}$ reflects the property of A_7, since $\sin\theta\sin\phi$ is positive for $0<\phi<\pi$ while negative for $\pi<\phi<2\pi$.

We estimate $A_{\rm UD}$, and its statistical errors for 820,000 top-quark signal events which is expected at the LHC one-year run with $L = 10\,{\rm fb}^{-1}$ after the event selection for the single lepton plus jets channel $pp \to t\bar{t} \to b\bar{b}WW \to b\bar{b}(\ell\nu)(jj)$ [31]. Taking into account the fraction[2] of $t \to bWg$ events that satisfy the kinematical cuts in eqs. (3.1) and (3.2), a sample of about 72,000 events for $t \to bWg$ followed by $W \to \ell\nu$ would be expected. In figure 7 (left), we display the distribution of the event sample in the z_1-z_2 plane. In order to see the T-odd asymmetries effectively, we divide the kinematical region into eight bins using the jet-energy ordering and the opening angle between the two jets in the top rest frame as

$$\begin{array}{llrllr}
\text{(I)} & z_1 > z_3 & \cos\theta_{bg} < -0.5, & \text{(V)} & z_1 < z_3 & \cos\theta_{bg} < -0.5,\\
\text{(II)} & z_1 > z_3 & -0.5 < \cos\theta_{bg} < 0, & \text{(VI)} & z_1 < z_3 & -0.5 < \cos\theta_{bg} < 0,\\
\text{(III)} & z_1 > z_3 & 0 < \cos\theta_{bg} < 0.5, & \text{(VII)} & z_1 < z_3 & 0 < \cos\theta_{bg} < 0.5,\\
\text{(IV)} & z_1 > z_3 & 0.5 < \cos\theta_{bg}, & \text{(VIII)} & z_1 < z_3 & 0.5 < \cos\theta_{bg}.
\end{array} \tag{3.5}$$

[2]For the total decay width of the top quark, we use the calculation including the $\mathcal{O}(\alpha_s)$ QCD corrections [26].

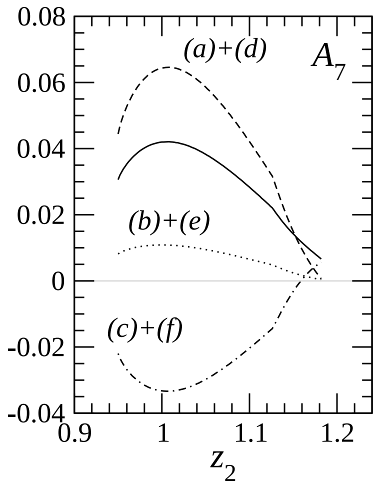

Figure 6: The contribution to the A_7 asymmetry for $0.55 < z_1 < z_{1\max}$ from the individual one-loop diagrams. (a)+(d), (b)+(e) and (c)+(f) contributions in Feynman gauge are plotted in dashed, dotted and dotted-dashed line. Total asymmetry is also plotted in solid line, as a reference.

In the figure, the number of events in each bin are given in an unit of thousands. As in figure 3, a large number of events is expected for the region where both z_1 and z_2 are large, namely (III) and (IV).

The top and middle plots in figure 7 (right) show the up-down asymmetries with expected statistical error-bars for each of the eight bins, for the LHC one-year run. The error is estimated from $\delta A = \sqrt{(1 - A^2)/N_{\rm sum}}$ for each bin. The magnitude of the asymmetry is larger for the (I)-(IV) bins than for the (V)-(VIII) bins, and increases with the opening angle θ_{bg}, as is expected from the z_1 and z_2 dependences of A_7 in figure 5. The asymmetry reaches 3% at the bin-(I) where, however, the event yield is not high.

In the bottom plot in figure 7 (right), we also consider the case where the top-pair productions are identified without a b-jet-tagging. In this case, instead of defining y-axis by the direction $\vec{q} \times \vec{p}_b$, we define the y-axis along $\vec{q} \times \vec{p}_{j_1}$, where p_{j_1} is the momentum of the jet whose energy is large than the other in the top-quark rest frame. This asymmetry corresponds to $A_{\rm UD}$ for $z_1 > z_3$ (top) minus $A_{\rm UD}$ for $z_1 < z_3$ (middle). Because of the cancellation, the magnitude of the asymmetry decreases, but it remains finite even without b-jet identifications.

4. Polarized top-quark decays

Although we have considered the decay of unpolarized top-quarks so far, the top-quarks produced singly by the electroweak interactions at hadron colliders or the top-quark pairs produced in e^+e^- colliders can be highly polarized. Therefore, it may be useful to analyze the polarized top-quark decay.

In this section, we show that, when a top-quark is polarized, i) there exists another type of T-odd observable, the angular correlation between the top-spin direction and the

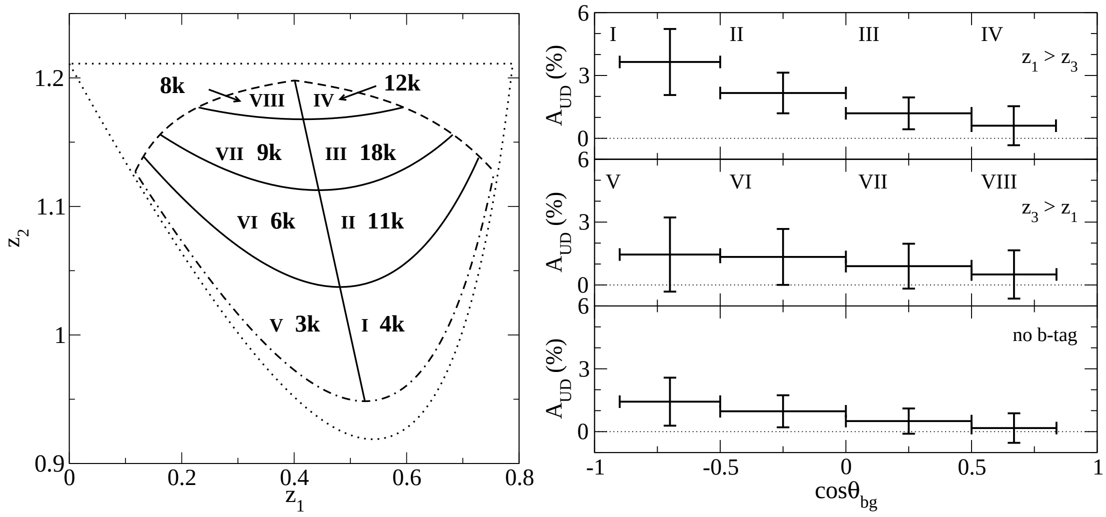

Figure 7: (Left) Estimation of the event yields for the LHC one-year run is shown in each bin defined in (3.5). (Right) Up-down asymmetries $A_{\rm UD}$ defined in eq. (3.4) for the eight bins (top and middle) and $A_{\rm UD}$ for the case without b-tagging (bottom). $\cos\theta_{bg}$ is the opening angle between the two jets in the top rest frame. Error bars are estimated for the expected event yields shown in the left figure.

top decay plane, and ii) the lepton angular distributions discussed in the previous section are modified.[3]

First, we discuss another type of T-odd observable in radiative decays of the polarized top-quarks, namely, the angular correlation between the top-quark spin and the decay plane.

We define the angles between the top-quark spin direction and the decay plane in the top-quark rest-frame as shown in figure 8. The z-axis is chosen along the W-momentum direction, and the x-axis is chosen along the $\vec{p}_b$ direction in the $(\vec{p}_b, \vec{p}_g)$ plane. The polar and azimuthal angles, θ_P and ϕ_P, respectively, define the direction of the top-quark spin $\vec{s}_t$.

The decay distribution is now characterized by the two angles as well as z_1 and z_2:

$$\begin{aligned}\frac{d\Gamma}{dz_1 dz_2 d\cos\theta_P d\phi_P} &= \frac{G_F \alpha_s m_t^3 x^2 |V_{tb}|^2 C_F}{64\sqrt{2}\pi^3} \\ &\times \Big[F_{P1} + F_{P2}\cos\theta_P + F_{P3}\sin\theta_P\cos\phi_P + F_{P4}\sin\theta_P\sin\phi_P \Big]. \quad (4.1)\end{aligned}$$

The structure functions $F_{P1-P4}(z_1, z_2)$ are obtained from the $t \to bWg$ matrix elements $\mathcal{M}_{\sigma_t}$, which are defined in eq. (2.8), but we now retain the top-quark helicity σ_t instead of

[3]We thank the referee of this article for pointing out the existence of another T-odd observable in the polarized top-quark decay, and suggesting its relation to the normal polarization in the top-quark pair-production.

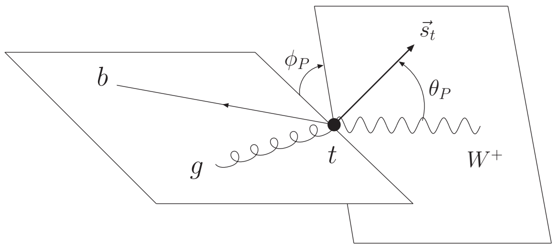

Figure 8: Schematic view of the coordinate system for the $t \to bW^+g$ decay, where the W^+ momentum direction in the top-quark rest-frame is chosen along the z-axis, with the top-quark's spin $\vec{s}_t$.

the W-helicity (λ):

$$F_{P1} = \frac{1}{2}\overline{\sum}\left(|\mathcal{M}_+|^2 + |\mathcal{M}_-|^2\right), \qquad F_{P3} = \frac{1}{2}\overline{\sum}\left(\mathcal{M}_+^*\mathcal{M}_- + \mathcal{M}_-^*\mathcal{M}_+\right),$$
$$F_{P2} = \frac{1}{2}\overline{\sum}\left(|\mathcal{M}_+|^2 - |\mathcal{M}_-|^2\right), \qquad F_{P4} = \frac{i}{2}\overline{\sum}\left(\mathcal{M}_+^*\mathcal{M}_- - \mathcal{M}_-^*\mathcal{M}_+\right). \tag{4.2}$$

The summation stands for the sum of the spins of all the particles but the top-quark, and the sum/average of colors. The spin-independent term F_{P1} is identical to F_1 in eq. (2.12), including the normalization factor. F_{P1} is T-even and P-even, while F_{P2} and F_{P3} are T-even and P-odd. F_{P4} is T-odd and P-even. The leading-order contribution to the functions F_{P1} to F_{P3} comes from the tree-level amplitudes. On the other hand, the leading-order contribution to F_{P4} comes from the interference between the tree amplitudes and the absorptive part of the one-loop amplitudes, just the same as $F_{7,8,9}$ in eq. (2.12). Note that F_{P4} is proportional to the expectation value of the triple product of the three vectors $\langle \vec{s}_t \cdot \vec{q} \times \vec{p}_b \rangle$, just like F_7 is proportional to $\langle \vec{s}_W \cdot \vec{q} \times \vec{p}_b \rangle$. The corresponding distribution for the anti-top-quark decay can be obtained by reversing the sign of F_{P2} and F_{P3} in eq. (4.1), when the CP is a good symmetry.

We define the ratios of the correlation functions F_i for $i = P2$-$P4$ to the spin-independent term F_{P1} as

$$A_i(z_2) = \int dz_1 F_i(z_1, z_2) \Big/ \int dz_1 F_{P1}(z_1, z_2). \tag{4.3}$$

Each correlation function corresponds to the expectation value of the component of the top-quark spin-vector as

$$\langle \vec{s}_t \rangle = \frac{1}{3}\left(A_{P3},\, A_{P4},\, A_{P2}\right). \tag{4.4}$$

In figure 9, the z_2 distributions of $A_{P2,P3}$ at the tree level and A_{P4} at the one-loop level are shown, where the three z_1 regions and the kinematical cuts are the same as those in figure 4. The T-even P-odd asymmetries A_{P2} and A_{P3} are as large as a few times 10% in magnitude, while the T-odd P-even asymmetry A_{P4} is less than 1%. This means that the top-quark spin lies almost in the decay plane, or, the decay plane tends to contain

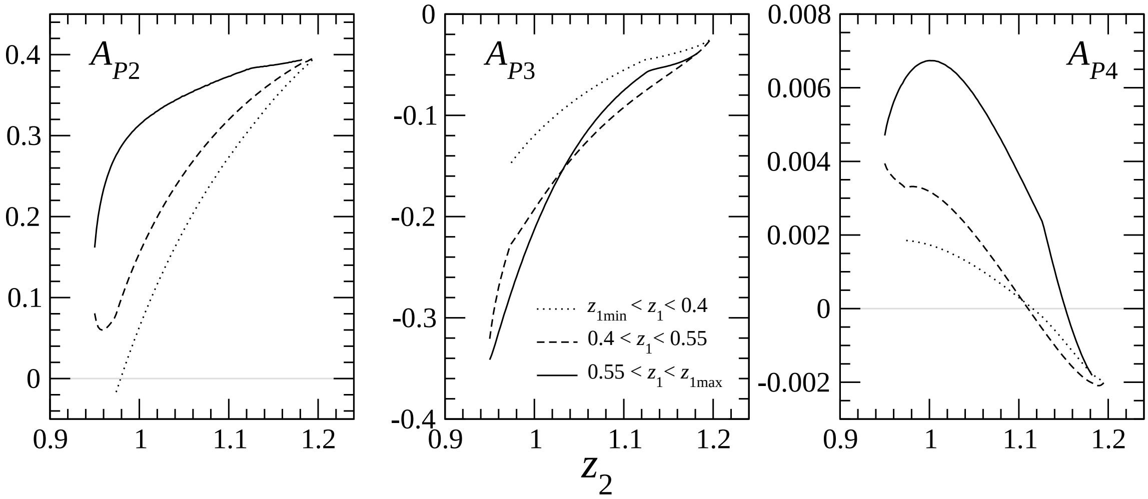

Figure 9: The z_2 distributions of the angular correlation functions defined in eq. (4.3), $A_{P2,P3}$ at the tree level and A_{P4} at the one-loop level, where the three z_1 regions and the kinematical cuts are the same as in figure 4.

the top-quark spin. The z_1 dependence of A_{P4} is similar to the T-odd lepton angular asymmetry A_7 in figure 5.

Next, we consider the T-odd lepton angular asymmetry A_7 again, but in the decay of polarized top-quarks. Since the degree of the normal polarization to the decay plane is quite small as shown in figure 9, for simplicity, the case that the top-quark spin lies in the decay plane, $\phi_P = 0°$, is considered. In figure 10, we show the A_7 asymmetry for $0.55 < z_1 < z_{1\mathrm{max}}$, where the spin direction of the top-quark is set at $\theta_P = 0°$ and $180°$. The asymmetry is enhanced when $\theta_P = 0°$, but reduced when $\theta_P = 180°$. It follows from the fact that the decay amplitude to the right-handed W-boson is larger for $\theta_P = 0°$ than for $\theta_P = 180°$.

Finally, we briefly mention T-odd effects induced by the absorptive part of the top-pair production amplitudes, which produce the normal polarization with respect to the scattering plane. The one-loop calculations have been done for e^+e^- and hadron colliders [16 − 21], however, the degree of polarization is estimated to be quite small.

We examine if the up-down asymmetry with respect to the decay plane of the top-quarks, studied in this paper, can contribute to the T-odd asymmetry about the scattering plane in the top-pair production process, when the production and decay processes are considered in total. When the top-quark has normal polarization with respect to the scattering plane, because the charged lepton prefers to be emitted in the direction of the top-quark spin, the expectation value of the inner product of the top-quark spin direction and the lepton direction $\langle \vec{s}_t \cdot \vec{p}_\ell \rangle$ is positive. On the other hand, considering the T-odd effects in the top-decay process, since the A_{P4} asymmetry in figure 9 is slightly positive, the expectation value of the triple product $\langle \vec{s}_t \cdot \vec{q} \times \vec{p}_b \rangle$ is slightly positive. In addition, since A_7 in figure 5 is positive, the expectation value of $\langle \vec{p}_\ell \cdot \vec{q} \times \vec{p}_b \rangle$ is also positive. Therefore, the T-odd effect in the top decay process gives positive correction to $\langle \vec{s}_t \cdot \vec{p}_\ell \rangle$, i.e. additive

JHEP12(2007)041

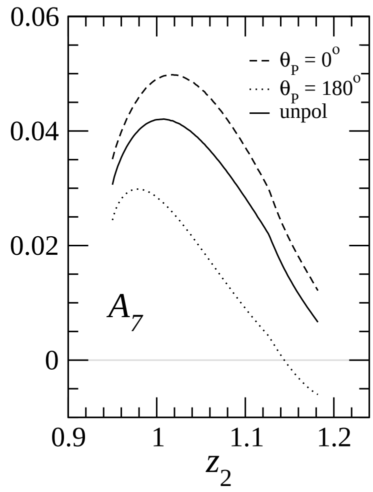

Figure 10: T-odd asymmetry A_7 for $0.55 < z_1 < z_{1\mathrm{max}}$ in the polarized top-quark decays. The direction of the polarization is parameterized from the W-momentum direction, $\theta_P = 0°$ (dashed) and $180°$ (dotted). As a reference, the unpolarized case is also plotted in solid line.

to the original asymmetry due to the T-odd polarization of the top-quark normal to the scattering plane. However the size should be negligible, because the degree of the normal polarization and the T-odd correlation A_{P4} are estimated to be very small.

Similarly, we find that the T-odd effect in the top-quark production process provides additive but negligible contribution to the T-odd asymmetry in the decay process with respect to the top decay plane.

5. Summary

In this article, we studied the top quark decay into a bottom quark and a W boson accompanied by one gluon emission, and calculated the absorptive part of the $t \to bWg$ decay amplitudes at the one-loop level. We then estimated the leading-order contribution to the T-odd asymmetries of the lepton angular distribution in the $t \to bWg$ decay followed by leptonic decay of the W boson.

For completeness, we also discussed the T-even asymmetries at the tree level $\mathcal{O}(\alpha_s)$, and found that the fraction to the right-handed W boson increases in the small W-boson energy region. As for the T-odd asymmetries, the largest asymmetry is predicted for A_7 at a few percent level, and the other asymmetries (A_8 and A_9) are found to be less than 1%.

We proposed a simple observable A_{UD}, the up-down asymmetry with respect to the top decay plane, which is proportional to A_7. The A_{UD} asymmetry is predicted to be at a few percent level, which may be confirmed at the LHC with $10\,\mathrm{fb}^{-1}$.

Before closing let us mention that, for the polarized top-quark decays, there exists another T-odd observable, the angular correlation between the top-quark spin direction and the top decay plane. However, the size of the T-odd correlation is less than 1%, which may be difficult to measure at future colliders.

Acknowledgments

K.H. wishes to thank E. Asakawa and M. Tanaka for discussions in the early stage of the investigation. K.M. and H.Y. thank the KEK theory group for the warm hospitality. We thank B. Jäger, Y. Kurihara and E. Senaha for discussions. This work is supported in part by the core university program of JSPS, and in part by the Grant-in-Aid for Scientific Research (Nos. 17540281, 18340060) of MEXT, Japan. The work of H.Y. is supported in part by a Research Fellowship of the Japan Society for the Promotion of Science.

A. $t \to bW^+g$ decay amplitudes

In this appendix, we outline our calculation of the amplitude for the $t \to bWg$ process. Note that we present the formalism in the $m_b = 0$ limit, because we performed the one-loop calculation only in this limit. The extension to the massive b-quark case will be given only for the tree-level calculation.

First, we expand the tensor $T^{\mu\alpha}$ in eq. (2.8) as

$$T^{\mu\alpha} = \sum_i a_i T_i^{\mu\alpha} \tag{A.1}$$

with the 20 basis tensors;

$$\begin{aligned}
T_{L1}^{\mu\alpha} &= g^{\mu\alpha} \not{\epsilon} P_-/m_t^2, & T_{R1}^{\mu\alpha} &= g^{\mu\alpha} P_+/m_t, \\
T_{L2}^{\mu\alpha} &= \gamma^\mu \gamma^\alpha \not{\epsilon} P_-/m_t^2, & T_{R2}^{\mu\alpha} &= \gamma^\mu \gamma^\alpha P_+/m_t, \\
T_{L3}^{\mu\alpha} &= p_t^\mu \gamma^\alpha P_-/m_t^2, & T_{R3}^{\mu\alpha} &= p_t^\mu \gamma^\alpha \not{\epsilon} P_+/m_t^3, \\
T_{L4}^{\mu\alpha} &= p_b^\mu \gamma^\alpha P_-/m_t^2, & T_{R4}^{\mu\alpha} &= p_b^\mu \gamma^\alpha \not{\epsilon} P_+/m_t^3, \\
T_{L5}^{\mu\alpha} &= \gamma^\mu p_t^\alpha P_-/m_t^2, & T_{R5}^{\mu\alpha} &= \gamma^\mu p_t^\alpha \not{\epsilon} P_+/m_t^3, \\
T_{L6}^{\mu\alpha} &= \gamma^\mu p_b^\alpha P_-/m_t^2, & T_{R6}^{\mu\alpha} &= \gamma^\mu p_b^\alpha \not{\epsilon} P_+/m_t^3, \\
T_{L7}^{\mu\alpha} &= p_t^\mu p_t^\alpha \not{\epsilon} P_-/m_t^4, & T_{R7}^{\mu\alpha} &= p_t^\mu p_t^\alpha P_+/m_t^3, \\
T_{L8}^{\mu\alpha} &= p_t^\mu p_b^\alpha \not{\epsilon} P_-/m_t^4, & T_{R8}^{\mu\alpha} &= p_t^\mu p_b^\alpha P_+/m_t^3, \\
T_{L9}^{\mu\alpha} &= p_b^\mu p_t^\alpha \not{\epsilon} P_-/m_t^4, & T_{R9}^{\mu\alpha} &= p_b^\mu p_t^\alpha P_+/m_t^3, \\
T_{L10}^{\mu\alpha} &= p_b^\mu p_b^\alpha \not{\epsilon} P_-/m_t^4, & T_{R10}^{\mu\alpha} &= p_b^\mu p_b^\alpha P_+/m_t^4
\end{aligned} \tag{A.2}$$

where the chiral-projection operators are $P_\pm = \frac{1}{2}(1 \pm \gamma_5)$. The summation runs for $i = \{L1\text{-}L10, R1\text{-}R10\}$. The coefficients a_i are calculated perturbatively,

$$a_i = b_i + i\alpha_s c_i + \cdots , \tag{A.3}$$

where b_i is the tree-level contribution, and c_i is the one-loop contribution to the absorptive part.

The 20 coefficients satisfy the following sum rules, because of the gauge invariance of QCD ($p_{g_\alpha} T^{\mu\alpha} = 0$),

$$\begin{aligned}
2(1 - y_2)a_{L2} + z_3 a_{L5} + y_2 a_{L6} + 2a_{R2} &= 0, \\
2a_{L2} + 2a_{R2} - z_3 a_{R5} - y_2 a_{R6} &= 0,
\end{aligned}$$

$$
\begin{aligned}
2a_{L1} - 2a_{L3} + z_3 a_{L7} + y_2 a_{L8} - 2a_{R3} &= 0, \\
2a_{L3} + 2a_{R1} + 2(1-y_2)a_{R3} + z_3 a_{R7} + y_2 a_{R8} &= 0, \\
2a_{L1} + 4a_{L2} + 2a_{L4} - z_3 a_{L9} - y_2 a_{L10} + 2a_{R4} &= 0, \\
2a_{L4} - 2a_{R1} - 4a_{R2} + 2(1-y_2)a_{R4} + z_3 a_{R9} + y_2 a_{R10} &= 0,
\end{aligned} \tag{A.4}
$$

where we defined $y_2 = 1 - z_2 + x^2$. In appendices A.1, A.2 and B, we present the following 14 coefficients; $i = L1$-$L4$,$L6$,$L8$,$L10$,$R1$-$R4$,$R6$,$R8$,$R10$. The remaining 6 coefficients; $i = L5$,$L7$,$L9$,$R5$,$R7$,$R9$ are then obtained from the above identities, eq. (A.4)[4].

Counting the number of the physical amplitudes, only the twelve among the 14 coefficients are independent [32, 4]. Using the Dirac matrix identity [32], the terms with $T^{\mu\alpha}_{L10}$ and $T^{\mu\alpha}_{R10}$ can be removed by the following replacements,

$$
\begin{aligned}
a_{L1} &\to a_{L1} + \frac{1}{2}(y_3 - z_1 z_2)a_{L10} - \frac{1}{2}z_1 a_{R10}, \\
a_{L2} &\to a_{L2} - \frac{1}{2}(y_3 - z_1 z_2)a_{L10} + \frac{1}{2}z_1 a_{R10}, \\
a_{L3} &\to a_{L3} - \frac{1}{2}z_2 y_3 a_{L10} - \frac{1}{2}y_3 a_{R10}, \\
a_{L4} &\to a_{L4} + \frac{1}{2}(z_2^2 - 2x^2)a_{L10} + \frac{1}{2}z_2 a_{R10}, \\
a_{L6} &\to a_{L6} + \frac{1}{2}\{(z_1 - z_2)z_2 + 2x^2\}a_{L10} + \frac{1}{2}(z_1 - z_2)a_{R10}, \\
a_{L8} &\to a_{L8} + z_2 a_{L10} + a_{R10}, \\
a_{R1} &\to a_{R1} + \frac{1}{2}z_1 x^2 a_{L10} + \frac{1}{2}y_3 a_{R10}, \\
a_{R2} &\to a_{R2} - \frac{1}{2}z_1 x^2 a_{L10} - \frac{1}{2}y_3 a_{R10}, \\
a_{R3} &\to a_{R3} + \frac{1}{2}y_3 a_{L10}, \\
a_{R4} &\to a_{R4} - \frac{1}{2}z_2 a_{L10} - a_{R10}, \\
a_{R6} &\to a_{R6} - \frac{1}{2}(z_1 - z_2)a_{L10} + a_{R10}, \\
a_{R8} &\to a_{R8} - x^2 a_{L10},
\end{aligned} \tag{A.5}
$$

with $y_3 = 1 - z_3 - x^2$.

A.1 Tree-level results

At the tree level, the amplitude has the contributions from two Feynman diagrams (figure 2),

$$
T^{\mu\alpha}_{\rm tree} = \gamma^\alpha \frac{1}{\not{p}_t - \not{q} + i\epsilon}\gamma^\mu P_- + \gamma^\mu P_- \frac{1}{\not{p}_t - \not{p}_g - m_t + i\epsilon}\gamma^\alpha. \tag{A.6}
$$

[4]To verify our results, we have calculated all the 20 coefficients independently and checked that these satisfy the eqs. (A.4).

The decomposition in terms of $T_i^{\mu\alpha}$ in (A.2) gives

$$b_{L1} = b_{L3} = -b_{R1} = 2x_b, \quad b_{L4} = -b_{L6} = 2x_t, \quad -b_{L2} = b_{R2} = x_t + x_b, \tag{A.7}$$

where $x_t \equiv m_t^2/(-2p_t \cdot p_g)$ and $x_b \equiv m_t^2/2p_b \cdot p_g$.

For the massive b-quark case, two more components,

$$T_{M1}^{\mu\alpha} = g^{\mu\alpha} P_-/m_t, \quad T_{M2}^{\mu\alpha} = \gamma^\mu \gamma^\alpha P_-/m_t, \tag{A.8}$$

with the coefficients $b_{M1} = 2yx_b$, $b_{M2} = -y(x_t + x_b)$ and $y = m_b/m_t$, must be added to eq. (A.1).

A.2 One-loop results

At the one-loop level, the absorptive part emerges from the six diagrams for the $t \to bWg$ decay, shown in figure 2. We write the one-loop coefficients in eq. (A.3) as the sum of these diagrammatic contributions,

$$c_i = c_i^{(a)} + c_i^{(b)} + c_i^{(c)} + c_i^{(d)} + c_i^{(e)} + c_i^{(f)}. \tag{A.9}$$

The analytic expressions of the coefficients are obtained for each diagram by performing the standard Feynman integrals. Our expression contains functions with a one-parameter integral, which can easily be evaluated.

In the next appendix, we also show the results of c_i in the loop scalar function method as an alternative expression. We checked that the numerical results of the two calculations agree completely.

With the color factor $C_F = 4/3$, $C_A = 3$ and $C_1 = C_F - C_A/2 = -1/6$, the one-loop coefficients for each diagram are found as below;

- diagram-(a)

$$-c_{L1}^{(a)} = 2c_{L2}^{(a)} = -c_{L3}^{(a)} = c_{R1}^{(a)} = -2c_{R2}^{(a)} = \frac{C_F}{2} x_b. \tag{A.10}$$

- diagram-(b)

$$-2c_{L1}^{(b)} = 4c_{L2}^{(b)} = -2c_{L3}^{(b)} = c_{L6}^{(b)} = 2c_{R1}^{(b)} = -4c_{R2}^{(b)} = C_1 x_b. \tag{A.11}$$

- diagram-(c)

$$-c_{L1}^{(c)} = 2c_{L2}^{(c)} = -c_{L3}^{(c)} = 2c_{L6}^{(c)} = c_{R1}^{(c)} = -2c_{R2}^{(c)} = \frac{C_A}{2} x_b \left(\ln \epsilon^2 + \ln x_b\right), \tag{A.12}$$

where $\epsilon = m_g/m_t$. The gluon mass m_g is introduced to regulate the IR singularity. We keep ϵ only in the singular parts and take the $\epsilon \to 0$ limit elsewhere.

- diagram-(d)

$$
\begin{aligned}
c_{L1}^{(d)} &= -2c_{L2}^{(d)} = -C_F\left[x_b(2-z_2)I_{10}-(3-z_2)I_{21}+\frac{2-y_2}{2}I_{22}\right],\\
c_{L3}^{(d)} &= -C_F\left[x_b(1-x^2)I_{10}-(1-x^2)I_{21}-\frac{y_2}{2}I_{22}-x^2y_2\left(I_{33}-I_{34}\right)\right],\\
c_{R1}^{(d)} &= -2c_{R2}^{(d)} = C_F\left[x_b(1-x^2)I_{10}-(2-x^2)I_{21}+\frac{2-y_2}{2}I_{22}\right],\\
c_{R3}^{(d)} &= C_F\left[I_{21}-I_{22}-y_2\left(I_{32}-I_{33}\right)\right].
\end{aligned}
\tag{A.13}
$$

Here, I_{mn} is defined by the integral

$$
I_{mn} = \int_0^1 \frac{t^n\,dt}{[1-z_2t+x^2t^2]^m}. \tag{A.14}
$$

- diagram-(e)

$$
\begin{aligned}
c_{L1}^{(e)} &= C_1\left[x_b\ln(z_1^2x_b)-(1+z_1)J_{110}+(z_2-x^2)J_{111}+\frac{y_2^2}{2}J_{213}-z_1L_2\right],\\
c_{L2}^{(e)} &= -\frac{1}{2}c_{L1}^{(e)}+\frac{C_1}{2}y_2\left[z_1(J_{121}-J_{122})+J_{211}-2J_{212}+\frac{2-y_2}{2}J_{213}\right],\\
c_{L3}^{(e)} &= C_1\Bigg[x_b\ln(z_1^2x_b)-I_{10}+y_2I_{21}-(1+z_1)J_{110}+(z_2-x^2)J_{111}+y_2^2J_{121}\\
&\quad +y_2J_{211}-\frac{y_2(2-y_2)}{2}J_{212}-z_1L_2\Bigg],\\
c_{L4}^{(e)} &= C_1\left[J_{110}-(z_2-x^2)J_{111}-y_2(1-z_2)J_{121}-\frac{y_2(y_2+2x^2)}{2}J_{122}\right],\\
c_{L6}^{(e)} &= -C_1\Bigg[2x_b+J_{110}-(1+x^2)J_{111}-y_2(2+z_1-z_2)J_{121}+\frac{y_2(2-y_2)}{2}J_{122}\\
&\quad +\frac{y_2(y_2+2x^2)}{2}J_{213}+\frac{z_1(z_1+y_2)}{z_1-y_2}L_2-\frac{2z_1^2y_2}{z_1-y_2}L_3\Bigg],\\
c_{L8}^{(e)} &= -C_1\left[4J_{111}-2y_2\left(J_{121}+J_{122}+2J_{212}+J_{213}\right)+y_2^2\left(J_{223}+2J_{314}\right)\right],\\
c_{L10}^{(e)} &= C_1y_2\left[2J_{122}-y_2\left(2J_{133}+J_{224}\right)\right],\\
c_{R1}^{(e)} &= -c_{L1}^{(e)}+C_1\left[I_{10}-y_2J_{110}-\frac{y_2^2}{2}\left(J_{212}-J_{213}\right)\right],\\
c_{R2}^{(e)} &= -\frac{1}{2}c_{R1}^{(e)}+\frac{C_1}{2}y_2\left[-2J_{111}+y_2J_{121}+(2-z_2)J_{211}-\frac{1+z_2-3x^2}{2}J_{212}\right],\\
c_{R3}^{(e)} &= -C_1y_2\left[J_{211}-J_{212}\right],\\
c_{R4}^{(e)} &= -C_1\left[J_{110}-J_{111}+y_2\left(J_{121}-J_{122}\right)\right],\\
c_{R6}^{(e)} &= C_1\left[J_{110}-2J_{111}+y_2\left(J_{121}+J_{212}\right)\right],\\
c_{R8}^{(e)} &= C_1\left[2J_{110}-2y_2\left(J_{121}+2J_{211}\right)+y_2^2\left(J_{222}+2J_{313}\right)\right],\\
c_{R10}^{(e)} &= -C_1y_2\left[4J_{121}-2J_{122}-y_2\left(2J_{132}+J_{223}\right)\right],
\end{aligned}
\tag{A.15}
$$

where $J_{mn\ell}$ and L_n are defined as

$$J_{mn\ell} = \int_0^1 \frac{t^\ell dt}{[1-z_2t+x^2t^2]^m[y_2t+z_1(1-t)]^n}, \tag{A.16}$$

$$L_n = \int_0^1 \frac{dt}{[y_2t+z_1(1-t)]^n}\ln\left(\frac{y_2t^2}{1-z_2t+x^2t^2}\right). \tag{A.17}$$

- diagram-(f)

$$\begin{aligned}
c_{L1}^{(f)} &= \frac{C_A}{2}\Bigg[x_b\ln(z_3^2x_b)-x_b-(1+z_3)J'_{110}+\frac{1+x^2}{2}J'_{111}+\frac{y_2(2+z_3)}{2}J'_{121}-\frac{z_2y_2}{2}J'_{122}\\
&\qquad +y_2J'_{212}-\frac{y_2(1+x^2)}{2}J'_{213}-\frac{z_3(y_2-3z_3)}{2(y_2-z_3)}L'_2-\frac{y_2z_3^2}{y_2-z_3}L'_3\Bigg],\\
c_{L2}^{(f)} &= \frac{C_A}{4}\Bigg[x_t\left(\ln\epsilon^2+\ln x_b\right)-x_b\ln(z_3^2x_b)+x_t+x_b+(1+z_3)J'_{110}-\frac{2-z_2+2x^2}{2}J'_{111}\\
&\qquad -\frac{y_2(z_2+z_3)}{2}J'_{121}+x^2y_2J'_{122}-\frac{y_2}{2}J'_{211}+\frac{x^2y_2}{2}J'_{213}+\frac{3}{2}(y_2+z_3)L'_2-y_2z_3L'_3\Bigg],\\
c_{L3}^{(f)} &= \frac{C_A}{2}\Bigg[x_b\ln(z_3^2x_b)-x_b-2z_3J'_{110}-\frac{z_2-2z_3-2x^2}{2}J'_{111}-y_2J'_{121}\\
&\qquad +\frac{y_2(3z_2+z_3-4x^2)}{2}J'_{122}-y_2(1-z_3)J'_{211}\\
&\qquad +\frac{y_2(3-2z_3-x^2)}{2}J'_{212}-\frac{z_3(y_2-3z_3)}{2(y_2-z_3)}L'_2-\frac{y_2z_3^2}{y_2-z_3}L'_3\Bigg],\\
c_{L4}^{(f)} &= -\frac{C_A}{2}\Bigg[x_t\left(\ln\epsilon^2+\ln x_b\right)+x_t+J'_{110}-(z_2-x^2)J'_{111}-\frac{y_2(2+z_2)}{2}J'_{121}\\
&\qquad +\frac{y_2(1+2z_2-x^2)}{2}J'_{122}+\frac{y_2(3y_2-z_3)}{2(y_2-z_3)}L'_2-\frac{y_2^2z_3}{y_2-z_3}L'_3\Bigg],\\
c_{L6}^{(f)} &= \frac{C_A}{2}\Bigg[\left(x_t-\frac{x_b}{2}\right)\left(\ln\epsilon^2+\ln x_b\right)+x_t+x_b+J'_{110}-\frac{1+z_2+x^2}{2}J'_{111}-\frac{y_2(z_2+z_3)}{2}J'_{121}\\
&\qquad +\frac{y_2(2z_2-z_3)}{2}J'_{122}-\frac{y_2(2-z_2)}{2}J'_{212}+\frac{y_2(1+x^2)}{2}J'_{213}+\frac{3y_2+2z_3}{2}L'_2-y_2z_3L'_3\Bigg],\\
c_{L8}^{(f)} &= \frac{C_A}{2}\left[4J'_{111}-2y_2\left(3J'_{122}+2J'_{212}+J'_{213}\right)+y_2^2\left(2J'_{133}+J'_{223}+J'_{224}+2J'_{314}\right)\right],\\
c_{L10}^{(f)} &= \frac{C_A}{2}y_2\left[2J'_{122}-y_2\left(2J'_{133}+J'_{224}\right)\right],\\
c_{R1}^{(f)} &= -c_{L1}^{(f)}+\frac{C_A}{2}\left[I_{10}-\frac{y_2}{2}\Big\{z_3(J'_{121}-J'_{122})+J'_{211}-(2+y_2)J'_{212}+J'_{213}\Big\}\right],\\
c_{R2}^{(f)} &= -c_{L2}^{(f)}+\frac{C_A}{4}\Bigg[I_{10}-\frac{y_2+4z_3}{2}J'_{110}-(y_2-2z_3)J'_{111}-\frac{y_2^2}{2}J'_{121}\\
&\qquad\qquad -\frac{y_2(1-z_2)}{2}J'_{211}-\frac{x^2y_2}{2}\left(2J'_{212}-J'_{213}\right)\Bigg],\\
c_{R3}^{(f)} &= -\frac{C_A}{2}\left[J'_{110}-J'_{111}-2y_2\left(J'_{121}-J'_{122}+J'_{211}-J'_{212}\right)\right],\\
c_{R4}^{(f)} &= \frac{C_A}{2}\left[J'_{110}-J'_{111}-2y_2\left(J'_{121}-J'_{122}\right)\right],
\end{aligned}$$

$$c_{R6}^{(f)} = -\frac{C_A}{2}\left[J'_{110} - 2J'_{111} + y_2\left(J'_{122} + J'_{212}\right)\right],$$
$$c_{R8}^{(f)} = -C_A\left[J'_{110} - 2y_2\left(J'_{121} + J'_{211}\right) + y_2^2\left(J'_{133} + J'_{223} + J'_{313}\right)\right],$$
$$c_{R10}^{(f)} = -\frac{C_A}{2}y_2\left[4J'_{121} - 2J'_{122} - y_2\left(2J'_{133} + J'_{223}\right)\right], \tag{A.18}$$

where $J'_{mn\ell}$ and L'_n are given by replacing z_1 to z_3 in $J_{mn\ell}$ and L_n in eq. (A.16) and eq. (A.17), respectively.

We note that the sum of the IR singular terms from the diagrams (c) and (f) is exactly proportional to the tree-level amplitude, therefore they do not contribute to the T-odd distribution.

B. Loop scalar functions

As a check of our calculation, we calculate the one-loop coefficients in terms of the loop scalar functions, the Passarino and Veltman's B, C, D functions [33].

For each diagram, we assign the masses and the momenta of the scalar function, following the FF notation [34], and take only the imaginary part of the functions. In this assignment we explicitly present the b-quark and gluon mass, $m_{b,g}$, for clarity, even though we take the massless limit in our analysis.

- diagram-(a) Defining $B_i = \mathrm{Im}\, B_i(m_g^2, m_b^2; p_{bg}^2)$ for i=0,1 with $p_{bg}^2 = (p_b + p_g)^2$, the coefficients are expressed as

$$-c_{L1}^{(a)} = 2c_{L2}^{(a)} = -c_{L3}^{(a)} = c_{R1}^{(a)} = -2c_{R2}^{(a)} = C_F x_b\big[B_0 + B_1\big]/\pi. \tag{B.1}$$

- diagram-(b) Defining $C_i^{(b)} = \mathrm{Im}\, C_i(m_g^2, m_b^2, m_b^2; p_{bg}^2, p_g^2, p_b^2)$ for i=0,11,12,21-24, the coefficients are expressed as

$$\begin{aligned}-c_{L1}^{(b)} &= 2c_{L2}^{(b)} = -c_{L3}^{(b)} = c_{R1}^{(b)} = -2c_{R2}^{(b)} \\ &= C_1\big[-C_0 - 2C_{11} + C_{12} - C_{21} + C_{23} - 2C_{24}/p_{bg}^2\big]\, m_t^2/\pi, \\ c_{L6}^{(b)} &= C_1\big[-C_0 - 2C_{11} + C_{12} - C_{21} + C_{23}\big]\, m_t^2/\pi.\end{aligned} \tag{B.2}$$

- diagram-(c) Defining $C_i^{(c)} = \mathrm{Im}\, C_i(m_g^2, m_b^2, m_g^2; p_{bg}^2, p_b^2, p_g^2)$ for i=0,11,12,21-24, the coefficients are expressed as

$$\begin{aligned}-c_{L1}^{(c)} &= 2c_{L2}^{(c)} = -c_{L3}^{(c)} = c_{R1}^{(c)} = -2c_{R2}^{(c)} \\ &= C_A\big[C_0 - C_{11} - 2C_{21} + 2C_{23} - 12C_{24}/p_{bg}^2\big]\, m_t^2/4\pi, \\ c_{L6}^{(c)} &= C_A\big[2C_0 + 4C_{11} - 3C_{12} + 2C_{21} - 2C_{23}\big]\, m_t^2/4\pi.\end{aligned} \tag{B.3}$$

- diagram-(d) Defining $C_i^{(d)} = \mathrm{Im}\, C_i(m_g^2, m_t^2, m_b^2; p_t^2, q^2, p_{bg}^2)$ for i=0,11,12,21-24, the coefficients are expressed as

$$c_{L1}^{(d)} = -\,2c_{L2}^{(d)}$$

$$
\begin{aligned}
&= -\,C_F x_b\big[-(2-z_2)C_0-(3-z_2)C_{11}+(z_2-x^2)C_{12}-C_{21}\\
&\quad -x^2C_{22}+z_2C_{23}-2C_{24}/m_t^2\big]\,m_t^2/\pi,\\
c_{L3}^{(d)} &= -\,C_F x_b\big[-(1-x^2)(C_0+C_{11})-x^2(C_{22}-C_{23})-2C_{24}/m_t^2\big]\,m_t^2/\pi,\\
c_{R1}^{(d)} &= -\,2c_{R2}^{(d)}\\
&= -\,C_F x_b\big[(1-x^2)C_0+(2-x^2)C_{11}-(z_2-x^2)C_{12}+C_{21}\\
&\quad +x^2C_{22}-z_2C_{23}+2C_{24}/m_t^2\big]\,m_t^2/\pi,\\
c_{R3}^{(d)} &= -\,C_F x_b\big[-C_{11}+C_{12}-C_{21}+C_{23}\big]\,m_t^2/\pi.
\end{aligned}
\tag{B.4}
$$

- diagram-(e) Defining $D_i^{(e)} = \mathrm{Im}\,D_i(m_g^2, m_t^2, m_b^2, m_b^2;\, p_t^2, q^2, p_g^2, p_b^2, p_{bg}^2, (q+p_g)^2)$ for i=0,11-13,21-27,31-313, the coefficients are expressed as

$$
\begin{aligned}
c_{L1}^{(e)} =& C_1\big[z_1D_0+(1+z_1)D_{11}-D_{12}+2(D_{27}+D_{312}-D_{313})/m_t^2\big]\,m_t^4/\pi,\\
c_{L2}^{(e)} =& C_1\big[-z_1D_0-(1+z_1)D_{11}+D_{12}+D_{21}+(z_2-x^2)D_{22}-(1-z_2+x^2)D_{23}-2D_{24}\\
&+z_1D_{25}-(z_2-z_3-2x^2)D_{26}-2D_{27}/m_t^2-x^2D_{32}-D_{34}+D_{35}+z_2D_{36}\\
&-z_3D_{37}-(1-z_1-2x^2)D_{38}+(1-z_1-x^2)D_{39}-(z_2-z_3)D_{310}\\
&-6(D_{312}-D_{313})/m_t^2\big]\,m_t^4/2\pi,\\
c_{L3}^{(e)} =& C_1\big[z_1D_0+(1+2z_1)D_{11}+(1-z_1-2z_2+2x^2)D_{12}-(1-z_2+x^2)(2D_{13}-D_{23})\\
&+(2+z_1)D_{21}+x^2D_{22}+(1-z_1-3z_2+2x^2)D_{24}-(4-2z_2+x^2)D_{25}\\
&+(2z_2-3x^2)D_{26}+D_{31}-z_2D_{34}-(1+z_3)D_{35}+x^2(D_{36}-D_{38})+z_3D_{37}\\
&-(1-z_1-x^2)D_{39}+(1-z_1+z_2-x^2)D_{310}+4(D_{27}+D_{311}-D_{313})/m_t^2\big]\,m_t^4/\pi,\\
c_{L4}^{(e)} =& C_1\big[-D_{11}+(z_2-x^2)D_{12}+(1-z_2+x^2)D_{13}-D_{21}-x^2D_{22}+z_2D_{24}+D_{25}\\
&-(z_2-x^2)D_{26}-2(D_{27}+D_{313})/m_t^2\big]\,m_t^4/\pi,\\
c_{L6}^{(e)} =& C_1\big[D_{11}+(1-2z_2+x^2)D_{12}+(z_2-z_3-x^2)D_{13}+2D_{21}+x^2D_{22}\\
&-(1-z_2+x^2)D_{23}-2z_2D_{24}+(z_1-z_3)D_{25}+(1-z_1)D_{26}+D_{35}-z_3D_{37}\\
&+x^2D_{38}+(1-z_1-x^2)D_{39}-z_2D_{310}+2(D_{27}-D_{312}+3D_{313})/m_t^2\big]\,m_t^4/\pi,\\
c_{L8}^{(e)} =& C_1\big[2(D_{12}-D_{13}+D_{24})+D_{22}+D_{23}-D_{25}-3D_{26}+D_{36}-D_{38}+D_{39}-D_{310}\big]2m_t^4/\pi,\\
c_{L10}^{(e)} =& C_1\big[-D_{23}+D_{26}+D_{38}-D_{39}\big]\,2m_t^4/\pi,\\
c_{R1}^{(e)} =& C_1\big[-z_1D_0-(2z_1+z_2-x^2)D_{11}-(1-z_1-2z_2+2x^2)D_{12}+(1-z_2+x^2)D_{13}\\
&-D_{21}-x^2D_{22}+z_2D_{24}+z_3D_{25}-(1-z_1-x^2)D_{26}\\
&-2(2D_{27}+D_{311}-D_{313})/m_t^2\big]\,m_t^4/\pi,\\
c_{R2}^{(e)} =& C_1\big[z_1D_0+(2z_1+z_2-x^2)D_{11}+(1-z_1-2z_2+2x^2)D_{12}+(2-z_2)D_{21}\\
&-(1-z_2+x^2)(D_{13}-D_{23})-(z_2-2x^2)(D_{24}-D_{26})-(3-2z_2+x^2)D_{25}\\
&+D_{31}-z_2D_{34}-(1+z_3)D_{35}+x^2(D_{36}-D_{38})+z_3D_{37}-(1-z_1-x^2)D_{39}\\
&+(1-z_1+z_2-x^2)D_{310}+2(2D_{27}+3D_{311}-3D_{313})/m_t^2\big]\,m_t^4/2\pi,\\
c_{R3}^{(e)} =& C_1\big[-D_{21}+D_{24}+D_{25}-D_{26}\big]\,m_t^4/\pi,
\end{aligned}
$$

$$
\begin{aligned}
c_{R4}^{(e)} =&C_1\big[D_{11}-D_{12}-D_{25}+D_{26}\big]\,m_t^4/\pi,\\
c_{R6}^{(e)} =&C_1\big[-D_{11}+2D_{12}-D_{13}+D_{24}-D_{26}\big]\,m_t^4/\pi,\\
c_{R8}^{(e)} =&C_1\big[-D_{11}+D_{13}-2D_{21}-D_{23}+3D_{25}-D_{34}-D_{39}+2D_{310}\big]\,2m_t^4/\pi,\\
c_{R10}^{(e)} =&C_1\big[D_{23}-2D_{25}+D_{26}+D_{39}-D_{310}\big]\,2m_t^4/\pi.
\end{aligned}
\tag{B.5}
$$

- diagram-(f) Defining $D_i^{(f)} = \mathrm{Im}\,D_i(m_g^2,m_t^2,m_b^2,m_g^2;\,p_t^2,q^2,p_b^2,p_g^2,p_{bg}^2,(q+p_b)^2)$ for i=0,11-13,21-27,31-313, the coefficients are expressed as

$$
\begin{aligned}
c_{L1}^{(f)} =&-C_A\big[-2z_3D_0-2(1+z_3)D_{11}-(2-3z_2+2x^2)D_{12}+(2+z_1-2z_2+2x^2)D_{13}\\
&-3D_{21}+(z_2-3x^2)D_{22}-(2-3z_2)D_{24}+3z_1D_{25}+(3-2z_1-3z_2+3x^2)D_{26}\\
&-x^2D_{32}-D_{34}+z_2D_{36}-(1-z_3-x^2)D_{38}+z_1D_{310}-2(2D_{27}+D_{312})/m_t^2\big]\\
&\times m_t^4/4\pi,\\
c_{L2}^{(f)} =&-C_A\big[2z_3D_0+2(1+z_3)D_{11}+(3-4z_2+3x^2)D_{12}-(2+z_1-2z_2+2x^2)D_{13}\\
&+5D_{21}+3x^2D_{22}-4z_2D_{24}-5z_1D_{25}+4(1-z_3-x^2)D_{26}+6D_{27}/m_t^2\big]m_t^4/8\pi,\\
c_{L3}^{(f)} =&-C_A\big[-2z_3(D_0+2D_{11})+(z_3-z_1)D_{12}+z_1D_{13}-(1+2z_3)D_{21}-3x^2D_{22}\\
&+2(1-z_1+x^2)D_{24}-2(1-2z_1-z_2+x^2)D_{25}-(1-z_3-x^2)(3D_{26}+D_{310})\\
&-D_{31}+z_2D_{34}+z_1D_{35}-x^2D_{36}-2(7D_{27}+5D_{311})/m_t^2\big]\,m_t^4/4\pi,\\
c_{L4}^{(f)} =&-C_A\big[-2D_{11}+2(z_2-x^2)D_{12}+(1-z_2+x^2)(D_{13}+D_{23})-2D_{21}-2x^2D_{22}\\
&+2z_2D_{24}+(2-3z_2)D_{25}+(z_2+2x^2)D_{26}+D_{35}-z_1D_{37}+x^2D_{38}\\
&+(1-z_3-x^2)D_{39}-z_2D_{310}-2(2D_{27}-5D_{313})/m_t^2\big]\,m_t^4/4\pi,\\
c_{L6}^{(f)} =&-C_A\big[2D_{11}+(3-5z_2+3x^2)D_{12}-2(z_1-z_2+x^2)D_{13}+4D_{21}-(z_2-4x^2)D_{22}\\
&+z_1D_{23}+(2-5z_2)D_{24}-2(1+2z_1-z_2)D_{25}-(3-2z_1-4z_2+5x^2)D_{26}\\
&+x^2D_{32}+D_{34}-D_{35}-z_2D_{36}+z_1D_{37}+(1-z_3-2x^2)D_{38}-(1-z_3-x^2)D_{39}\\
&-(z_1-z_2)D_{310}+2(3D_{27}+D_{312}-D_{313})/m_t^2\big]\,m_t^4/4\pi,\\
c_{L8}^{(f)} =&-C_A\big[2(D_{12}-D_{13}+D_{24}-D_{25})+D_{22}-D_{26}+D_{36}-D_{310}\big]\,m_t^4/\pi,\\
c_{L10}^{(f)} =&-C_A\big[D_{23}-D_{26}-D_{38}+D_{39}\big]\,m_t^4/\pi,\\
c_{R1}^{(f)} =&-C_A\big[2z_3D_0+2(1+2z_3)D_{11}-(2-2z_1+z_2-2x^2)D_{12}-(2+z_1-2z_2+2x^2)D_{13}\\
&+5D_{21}+3x^2D_{22}-4(z_2D_{24}+z_1D_{25})+(1-z_3-x^2)(3D_{26}+D_{310})+D_{31}\\
&-z_2D_{34}-z_1D_{35}+x^2D_{36}+2(5D_{27}+D_{311})/m_t^2\big]\,m_t^4/4\pi,\\
c_{R2}^{(f)} =&-C_A\big[-2z_3D_0-(11-4z_1-5z_2+x^2)D_{11}+(2-2z_1+z_2-2x^2)D_{12}\\
&+(2+z_1-2z_2+2x^2)D_{13}-(5+z_2)D_{21}-5x^2D_{22}+(5z_2+2x^2)D_{24}\\
&-(1-6z_1-z_2+x^2)D_{25}-5(1-z_3-x^2)D_{26}-12D_{27}/m_t^2\big]\,m_t^4/8\pi,\\
c_{R3}^{(f)} =&-C_A\big[-D_{11}+D_{12}-2(D_{21}-D_{24})\big]\,m_t^4/2\pi,\\
c_{R4}^{(f)} =&-C_A\big[D_{11}-D_{12}+2(D_{25}-D_{26})\big]\,m_t^4/2\pi,\\
c_{R6}^{(f)} =&-C_A\big[-D_{11}+2D_{12}-D_{13}+D_{24}-D_{25}\big]\,m_t^4/2\pi,
\end{aligned}
$$

$$
\begin{aligned}
c_{R8}^{(f)} &= -\, C_A \big[-D_{11} + D_{13} - 2(D_{21} - D_{25}) - D_{34} + D_{35} \big]\, m_t^4/\pi, \\
c_{R10}^{(f)} &= -\, C_A \big[-D_{23} + 2D_{25} - D_{26} - D_{37} + D_{310} \big]\, m_t^4/\pi.
\end{aligned} \tag{B.6}
$$

References

[1] A. De Rujula, R. Petronzio and B. Lautrup, *On the challenge of measuring the color charge of gluons*, *Nucl. Phys.* **B 146** (1978) 50.

[2] J.G. Korner, G. Kramer, G. Schierholz, K. Fabricius and I. Schmitt, *A null result in massless QCD: beam-event asymmetry in $e^+e^- \to q\bar{q}g$ with longitudinally polarized beams*, *Phys. Lett.* **B 94** (1980) 207;
K. Fabricius, I. Schmitt, G. Kramer and G. Schierholz, *How to measure the color charge of gluons*, *Phys. Rev. Lett.* **45** (1980) 867.

[3] K. Hagiwara, K. Hikasa and N. Kai, *Measuring three gluon coupling in semiinclusive neutrino and anti-neutrino scattering*, *Phys. Rev. Lett.* **47** (1981) 983.

[4] K. Hagiwara, K. Hikasa and N. Kai, *Time reversal odd asymmetry in semiinclusive leptoproduction in quantum chromodynamics*, *Phys. Rev.* **D 27** (1983) 84.

[5] B. Pire and J.P. Ralston, *Single spin asymmetries in the Drell-Yan process*, *Phys. Rev.* **D 28** (1983) 260.

[6] K. Hagiwara, K.-i. Hikasa and N. Kai, *Parity odd asymmetries in W jet events at hadron colliders*, *Phys. Rev. Lett.* **52** (1984) 1076.

[7] K. Hagiwara, T. Kuruma and Y. Yamada, *Three jet distributions from the one loop Zgg vertex at e^+e^- colliders*, *Nucl. Phys.* **B 358** (1991) 80.

[8] K. Hagiwara, T. Kuruma and Y. Yamada, *Probing the one loop Zgg vertex at hadron colliders*, *Nucl. Phys.* **B 369** (1992) 171.

[9] A. Brandenburg, L.J. Dixon and Y. Shadmi, *Event handedness in e^+e^- annihilation to three jets*, *Phys. Rev.* **D 53** (1996) 1264 [hep-ph/9505355].

[10] A. De Rujula, J.M. Kaplan and E. De Rafael, *Elastic scattering of electrons from polarized protons and inelastic electron scattering experiments*, *Nucl. Phys.* **B 35** (1971) 365.

[11] K. Hagiwara, K.-i. Hikasa and H. Yokoya, *Parity-odd asymmetries in W-jet events at the Tevatron*, *Phys. Rev. Lett.* **97** (2006) 221802 [hep-ph/0604208].

[12] M. Ahmed and T. Gehrmann, *Azimuthal asymmetries in hadronic final states at HERA*, *Phys. Lett.* **B 465** (1999) 297 [hep-ph/9906503].

[13] R.D. Carlitz and R.S. Willey, *Single spin asymmetries in muon pair production*, *Phys. Rev.* **D 45** (1992) 2323.

[14] H. Yokoya, *Single longitudinal-spin asymmetries in lepton-pair production at RHIC and J-PARC*, *Prog. Theor. Phys.* **118** (2007) 371.

[15] J.G. Korner, B. Melic and Z. Merebashvili, *Analyticity, crossing and the absorptive parts of the one- loop contributions to the quark-quark-gluon gauge boson four-point function*, *Phys. Rev.* **D 62** (2000) 096011 [hep-ph/0002302].

[16] J.H. Kuhn, A. Reiter and P.M. Zerwas, *Z decays to top quarks*, *Nucl. Phys.* **B 272** (1986) 560.

[17] G.L. Kane, G.A. Ladinsky and C.P. Yuan, *Using the top quark for testing standard model polarization and CP predictions*, *Phys. Rev.* **D 45** (1992) 124.

[18] W. Bernreuther, J.P. Ma and T. Schroder, *Top quark polarization and T odd spin correlations as tools for testing (non)standard model predictions*, *Phys. Lett.* **B 297** (1992) 318.

[19] W. Bernreuther, A. Brandenburg and P. Uwer, *Transverse polarization of top quark pairs at the Tevatron and the Large Hadron Collider*, *Phys. Lett.* **B 368** (1996) 153 [hep-ph/9510300].

[20] W.G.D. Dharmaratna and G.R. Goldstein, *Single quark polarization in quantum chromodynamics subprocesses*, *Phys. Rev.* **D 53** (1996) 1073.

[21] A. Brandenburg, M. Flesch and P. Uwer, *The spin density matrix of top quark pairs produced in electron positron annihilation including QCD radiative corrections*, *Phys. Rev.* **D 59** (1999) 014001 [hep-ph/9806306].

[22] SLD collaboration, K. Abe et al., *First measurement of the T-odd correlation between the Z_0 spin and the three-jet plane orientation in polarized Z_0 decays to three jets*, *Phys. Rev. Lett.* **75** (1995) 4173 [hep-ex/9510005].

[23] HERMES collaboration, A. Airapetian et al., *Observation of a single-spin azimuthal asymmetry in semi-inclusive pion electro-production*, *Phys. Rev. Lett.* **84** (2000) 4047 [hep-ex/9910062].

[24] ZEUS collaboration, S. Chekanov et al., *Measurement of azimuthal asymmetries in neutral current deep inelastic scattering at HERA*, *Eur. Phys. J.* **C 51** (2007) 289 [hep-ex/0608053].

[25] G. Bunce et al., *Lambda 0 hyperon polarization in inclusive production by* 300 *GeV protons on Beryllium*, *Phys. Rev. Lett.* **36** (1976) 1113;
S. Erhan et al., *Lambda0 polarization in proton proton interactions at* $\sqrt{s} = 53\,GeV$ *and* $62\,GeV$, *Phys. Lett.* **B 82** (1979) 301;
R608 collaboration, A.M. Smith et al., Λ_0 *polarization in proton proton interactions from* $S^1/2 = 31\,GeV$ *to* $62\,GeV$, *Phys. Lett.* **B 185** (1987) 209.

[26] A. Czarnecki and K. Melnikov, *Two-loop QCD corrections to top quark width*, *Nucl. Phys.* **B 544** (1999) 520 [hep-ph/9806244];
K.G. Chetyrkin, R. Harlander, T. Seidensticker and M. Steinhauser, *Second order QCD corrections to* $\Gamma(T \to WB)$, *Phys. Rev.* **D 60** (1999) 114015 [hep-ph/9906273].

[27] M. Fischer, S. Groote, J.G. Korner and M.C. Mauser, *Complete angular analysis of polarized top decay at* $O(\alpha_s)$, *Phys. Rev.* **D 65** (2002) 054036 [hep-ph/0101322].

[28] G. Couture, *Massive top quark decay with emission of a photon or a gluon*, *Phys. Rev.* **D 40** (1989) 2927;
V.D. Barger, A. Stange and W.Y. Keung, *Photon and gluon bremsstrahlung in heavy top quark decay*, *Phys. Rev.* **D 42** (1990) 1835.

[29] S. Mrenna and C.P. Yuan, *QCD radiative decay of the top quark produced in hadron collisions*, *Phys. Rev.* **D 46** (1992) 1007.

[30] D. Binosi and L. Theussl, *Jaxodraw: a graphical user interface for drawing Feynman diagrams*, *Comput. Phys. Commun.* **161** (2004) 76 [hep-ph/0309015].

[31] See *ATLAS detector and physics performance. Technical design report, volume* 2, chapter 18.

[32] M. Perrottet, *Invariant amplitudes for compton scattering of off-shell photons on polarized nucleons*, *Lett. Nuovo Cim.* **7** (1973) 915;
R.J. Gonsalves, *Invariant amplitudes for $q\bar{q}g$ final states in e^+e^- annihilation*, *Phys. Rev.* **D 34** (1986) 1316.

[33] G. Passarino and M.J.G. Veltman, *One loop corrections for e^+e^- annihilation into $\mu^+\mu^-$ in the Weinberg model*, *Nucl. Phys.* **B 160** (1979) 151.

[34] G.J. van Oldenborgh, *FF: a package to evaluate one loop Feynman diagrams*, *Comput. Phys. Commun.* **66** (1991) 1.